22nd International Symposium on Plasma Chemistry
July 5-10, 2015; Antwerp, Belgium

Arc structures in twin-cathode DC electric arc furnace

F. Aristizabal, F.P. Sainct, M.D.G. Evans and S. Coulombe

Plasma Processing Laboratory, Department of Chemical Engineering, McGill University, Montréal, Québec, Canada

Abstract: Arc structures in a twin-cathode electric arc furnace were studied using voltage and current measurements, and image analysis. Arc structure was determined by the number of separate arcs and number of attachment points on the anode. The probability of having two separate arcs depends on the electrode gap (distance between the cathodes and common anode). A memory effect in the transition between structures has been observed.

Keywords: electric arc furnace, twin-cathode, arc interaction

1. Introduction

Industrial applications of DC and AC electric arc furnaces (EAF) range from steelmaking and smelting processes [1] to municipal waste treatment [2]. In a typical two-electrodes arrangement (Fig. 1), the powered electrodes are mounted above the load to be treated. Two configurations are commonly used for DC EAF: 1) dual-electrode, where one electrode is the cathode while the other acts as the anode; or 2) twin-cathode, where both electrodes act as cathodes and the load acts as the anode. The first configuration offers the possibility to operate with non-conductive or poorly conductive loads, while the second leads to more stable arcs and higher heat transfer rates to the loads [3]. An interesting difference between these two configurations is that, due to the arcs' interaction via the Lorentz force, the arcs repel each other in the dual-electrode configuration, while they attract each other in the twin-cathode configuration [4]. This difference gives the twin-cathode configuration a significant advantage for industrial applications, i.e. reduced arcing to the walls of the EAF and better arc stability.

Another important aspect of the industrial EAF is that the electrodes are sized for a narrow range of operating current so as to minimize consumption rates [3]. One interesting potential avenue to enhance the range of operation is to use multiple electrodes arranged in a regular pattern, each operating at or near the optimal current density. The current could thus be adjusted by altering the number of electrodes lit. In a different application context and configuration, Watanabe and his team studied multi-phase AC arcs (12 electrodes) to obtain more uniform thermal plasma volumes [5].

This study reports on our first findings on the arcs' interaction dynamics with a twin-cathode EAF configuration. The main objective is to characterize the types of structures the interacting arcs form depending on the electrode gap (cathode-to-anode distance) and other operating parameters.

2. Experimental Setup

An actual photo (left) and schematic view (right) of the experimental setup used in this study are shown in Fig. 1. The main components are: 1) twin-cathode EAF and

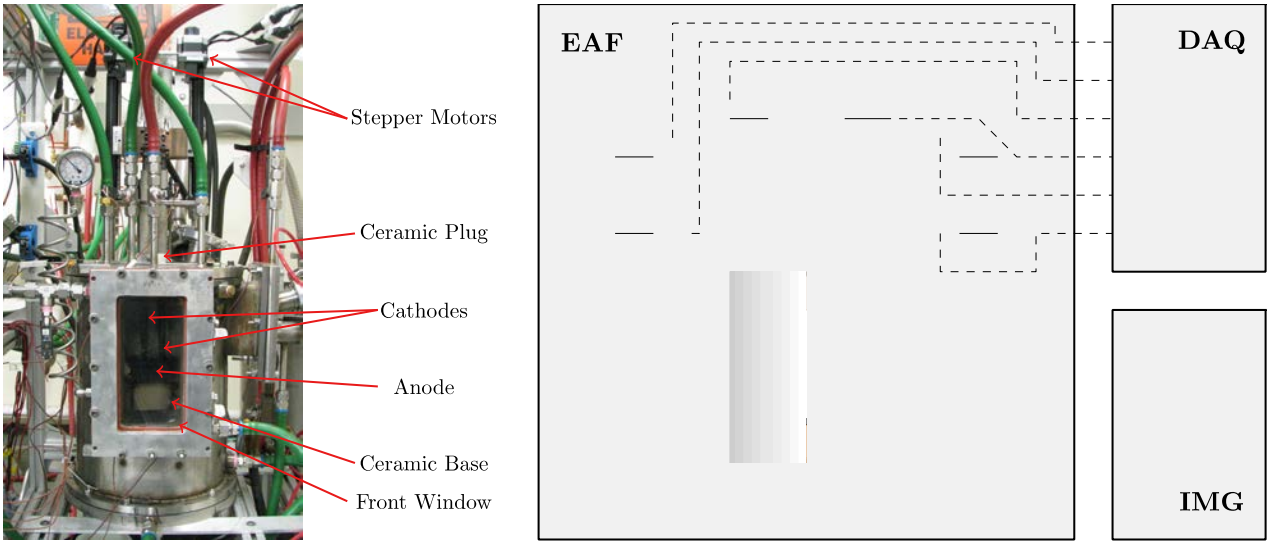

Fig. 1. Actual photo (left) and schematic view of the experimental setup (right).

power supplies, 2) data acquisition system (DAQ), and 3) images acquisition system (IMG).

The body of the furnace consists of a cylindrical stainless steel vessel, 25 cm in diameter and 38 cm in height, with a 12 cm by 23 cm rectangular quartz view port (front window) used for visualizing the arcing process. The EAF was configured for twin-cathode operation, i.e. two electrodes acting as cathodes (E_1 and E_2) and one common anode (AN). The cathodes are graphite rods (1.27 cm diameter) mounted on independent motorized linear displacement stages each having a total travel of 15.2 cm (XSlide, Velmex inc.). The cathodes are fed through a ceramic plug attached to the top plate to avoid electrical contact with the body of the EAF. The distance between the twin cathodes is 3.0 cm (center-to-center). The anode electrode consists of a 1.27 cm-thick, 15 x 15 cm^2 graphite plate placed on top of a ceramic base and connected to the power supplies through a copper feedthrough. Four power-regulated Miller rectifiers (SRH-444, Miller Electric Mfg) connected in series provide the DC power for each cathode. The anode and body of the EAF are grounded. Argon flowing at 7 L/min was used for all experiments.

The data acquisition system logs the voltage, current and position of each electrode in a computer for post-processing and analysis. The voltage drop between each cathode (V_1 and V_2) and the common anode is measured using a voltage divider. The current across each cathode (I_1 and I_2) is measured using a closed-loop Hall effect sensor (HCS 300A, HARTING). The cathode position is determined from the number of steps taken by the stepper motor with respect to the position at the beginning of the experiment. All experiments start with the cathodes put in contact with the anode; therefore the number of steps taken by a motor is proportional to the distance between the anode and the corresponding cathode.

The image acquisition system consists of a digital camera (Canon PowerShot S5 IS) mounted on a tripod 1 m away from the front window. A welding shield (shade 12) was placed between the EAF and the camera for protection and to avoid saturation of the sensor while recording videos.

3. Methodology

Voltage and current signals were sampled at 5 kHz. The current signals were post-processed using a zero-phase low-pass FIR filter with a pass band of 10 Hz and a stop band of 80 Hz. This process eliminates the natural 180 Hz frequencies from the power supplies. The signals were then down-sampled to 30 Hz to match the video frame rate. An example of raw signals and signals after filtering and down-sampling is shown in Fig. 2. This figure shows a typical current signal from the power supplies (red lines). A ~10 A variation around the mean value can be observed. Sampling the signal at a lower rate would transform the characteristic fluctuation of the power supply into noise. The filtered and down-sampled signal is shown in black in Fig. 2.

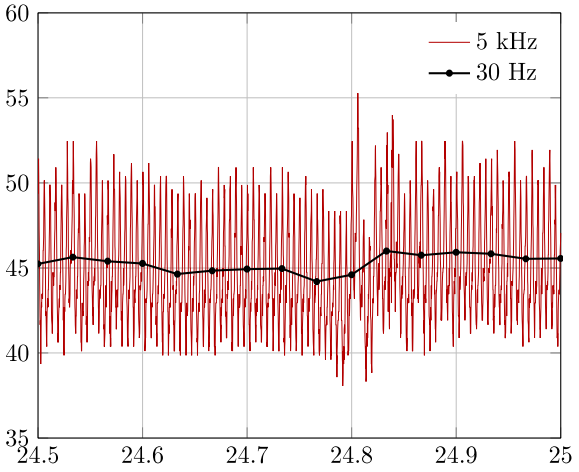

Fig. 2. Typical current signals, raw at 5 kHz (red) and filtered and down sampled to 30 Hz (black).

Videos of the arcs were acquired at 30 fps. Each frame was processed independently. Frame images are 640x480 pixels with three-color channels RGB (red, green and blue). Image processing techniques were used to determine: 1) electrode position, 2) arc structure and 3) arc length. Three different cases of processed images are shown in Fig. 3. The electrode position was obtained using thresholding on the blue channel to find the brightest spots near each cathode (higher green spots on

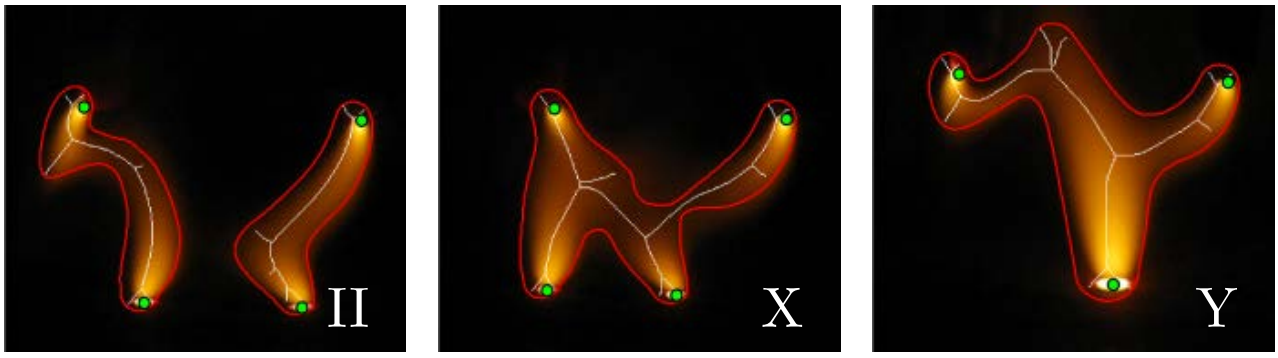

Fig. 3. Typical arc structures and image analysis steps.

Fig. 3.). The electrode position obtained from the camera was used to synchronize signals from the DAQ with the images acquired. Arc structure was obtained using thresholding and morphological operations (connected components) on the red channel and validated with the green channel (red lines in Fig. 3). This methodology allows image classification depending on the number of arcs detected; two separate arcs or a single merged arc. The bright spots on the anode were also counted (lower green spots in Fig. 3.); this is an indicator of the number of arc attachments. Arc length was determined using the skeleton morphological technique to estimate the distance between the bright spots near the cathodes and the attachment point on the anode (white lines in Fig. 3). The shortest distance between the cathode and anode spots was taken as the arc length.

4. Results and Discussion

The cathode-to-anode (electrode) gaps (d_1 and d_2) for a typical experiment are shown in Fig. 4. Each experiment was started with the electrodes in contact. After a minute of resistive heating the electrodes were raised in steps of 5 mm and each position was sampled during at least a minute. Displacements between 5 and 40 mm were sampled. The electrodes were then lowered in steps of 5 mm. Each experiment is divided in two parts depending on the direction of travel of the electrodes: raising or lowering. Only the times when both electrodes have the same gap are considered in the analysis.

The *V-I* characteristic curve for electrode 2 is presented in Fig. 5. Each color represents a different gap. The typical negative slope relation between voltage and current can be observed in this figure. The increase in voltage with electrode gap can also be distinguished in this figure.

Arc structure was determined using image analysis, depending on the number of arcs and attachment spots on the anode detected for a given image. Three main

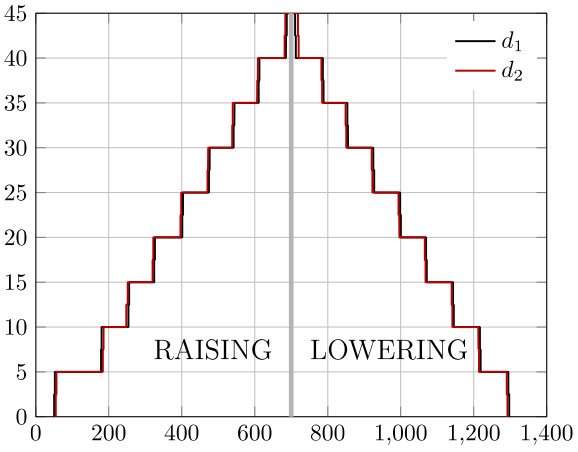

Fig. 4. Cathode-to-anode gaps recorded for a typical experiment.

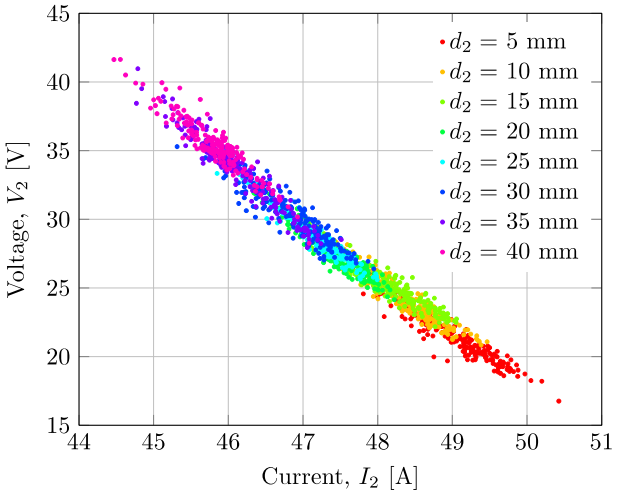

Fig. 5. *V-I* characteristic curve for electrode 2.

structures were identified in this study; examples of these are indicated in Fig. 3. The structures were classified as follows:

II: two separate arcs with two or more attachment points on the anode.

Y: a Y-shaped arc structure with a central bridging and a single attachment point on the anode.

X: a X-shaped arc structure with a central bridging and two (or more) attachment points on the anode.

For the rest of the analysis only two structures are considered. Structure X was assumed to be similar to structure II because both structures have two attachment points on the anode, indicating two electrically-separated arcs.

The probability or frequency of occurrence, *p(d)*, of structure II was quantified by counting the number of times structure II happens and dividing by the total number of frames at a given electrode gap. The average probability for structure II as a function of electrode gap is shown in Fig. 6. The error bars in this figure correspond to 95% confidence intervals (18 repeats). Dashed lines connecting the center points are included to ease the visualization.

For small cathode-to-anode gaps, two separated arcs tend to form. As the cathode-to-anode distance approaches the twin-cathodes' center-to-center distance (30 mm) the arcs have a higher tendency to form the Y structure and this, independently of the travel direction of the electrodes.

Fig. 6 also features an hysteresis which is indicative of a memory effect: Besides the normal tendency to form two arcs at small gaps and a merged arc at long gaps, the arcs demonstrate a preference for a given structure depending on the travel direction of the electrode. Raising the electrodes favors the persistence of structure II, while lowering the electrodes favors the persistence of a merged arc (structure Y). The persistence of one structure with respect to the other for a given electrode travel direction

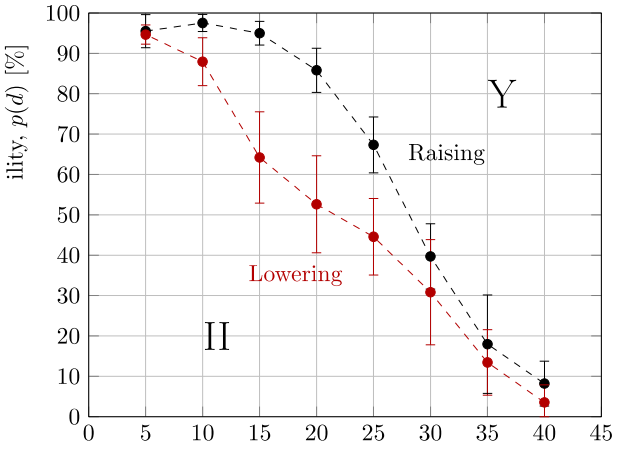

Fig. 6. Probability of occurrence of structure II as a function of electrode gap. Center-to-center distance between the two cathodes is 30 mm.

may simply be associated with the overlap of the domain of existence for both structures. It is suspected that arc fluctuations associated with the power supply noise, turbulent flow conditions, and/or electrode jets may trigger the transitions from one structure to another. This opens the door to a control of the arc structure by modulation of the arc power.

5. Conclusion

A preliminary study of arc structures formed in a laboratory-scale twin-cathode DC EAF was performed. The *V-I* curves obtained while varying the cathode-to-anode distances revealed the characteristic arc behavior, with a continuous merging of the data obtained at various electrode distances. Three characteristic structures were observed: two separated arcs (II), merged arcs with a single anode attachment point (Y), and merged arcs with two separate anode attachment points (X). Structure II tends to prevail at cathode-to-anode distance smaller than the spacing between the twin cathodes, while structure Y tends to be more frequently observed at larger spacing. Cycling the cathode-to-anode spacing revealed a memory effect where a given structure persists longer depending on the cycling direction.

6. Acknowledgments

The authors acknowledge the financial support provided by MITACS, NSERC, FRQNT and McGill University, and the technical and financial support provided by PyroGenesis Canada Inc.

7. References

[1] R. Jones, Q. Reynolds, T. Curr, and D. Sager, Some myths about DC arc furnaces, *Journal of the Southern African Institute of Mining and Metallurgy*, 111 (2011), pp. 665 – 674

[2] G. C. Young, Municipal solid waste to energy conversion processes: economic, technical, and renewable comparisons, *John Wiley & Sons*, 2010

[3] Q. Reynolds and R. Jones, Twin-electrode DC smelting furnaces - theory and photographic testwork, *Minerals Engineering*, 19 (2006), pp. 325 – 333

[4] Q. Reynolds. The dual-electrode DC arc furnace-modelling insights. *Journal of the Southern African Institute of Mining and Metallurgy*, 111 (2011), pp. 697-704

[5] M. Tanaka, T. Ikeba, Y. Liu, S. Choi and T. Watanabe, Investigation of electrode erosion mechanism of multi-phase AC arc by high-speed video camera, *Journal of Physics: Conference Series*, 441 (2013), p. 012015